

Characterization of Damage Behavior During Hot Forging



Ahmed A. M. Okasha, Hussein M. A. Hussein, Mostafa Shazly,
and Osama M. Dawood

Abstract During hot forging process, surface cracks may be deformed in several positions. These cracks may have repeated during production process which may have an impact on the life of the product. Deforming conditions (forming temperature, strain rate, and stress triaxiality) may be responsible for these cracks' formation. This work is an effort to study the effects of the forming conditions on the damage behavior and develop models using the stress–strain curves of steel C45 material as a case study. It is found that; Raising the formation temperature at constant strain rates reduces damage initiation strain and fractural stress but increases fractural strain. Also increasing the strain rates leads to reduction of the fractural strain (complete fracture), at the same time causing increase of the flow stresses and the damage initiation strain (at ultimate point). It was observed that increasing the stress triaxiality reduced the damage strains (initiation and complete fracture). A finite element model on a tension test was conducted to locate and explain the damage initiation and complete fracture in a cutting plane that passes through the necking zone and to show the damaging effect on the material strength. It was noticed that the damage started at the central elements and the damage reduced the material stiffness after damage initiation.

Keywords Ductile damage · Fractural strain · Forging temperature · Strain rate · Stress triaxiality

A. A. M. Okasha (✉) · H. M. A. Hussein · O. M. Dawood
Mechanical Engineering Dept., Faculty of Engineering, Helwan University, Cairo, Egypt

H. M. A. Hussein
e-mail: husein@h-eng.helwan.edu.eg

H. M. A. Hussein
Mechanical Engineering Dept., Ahram Canadian Univ., 6th of October City, Giza, Egypt

M. Shazly
Mechanical Engineering Dept., The British University in Egypt, Elshorouk City 11187, Egypt
e-mail: mostafa.shazly@bue.edu.eg

1 Introduction

Metal forming processes may experience cracks (or fractures) during these processes due to the accumulation of plastic deformation especially at high strain rates with extended strain and relatively low temperatures. The cracking phenomena are related to -so called- material damage models which can be classified generally into brittle (cleavage), ductile, intergranular, and fatigue damages [1, 2].

The ductile damage model proposes from macroscopic point of view that the damage initiation starts at the instability zone (necking zone) [2, 3]. Also, this model proposes that the damage occurs in six steps; (1) inclusions or/and second phase in a ductile matrix, (2) void nucleation around the second phase or/and inclusions, (3) void growth, (4) strain localization between voids, (5) necking between voids, and (6) void coalescence and fracture [2, 4].

It is well-known that the necking starts at the ultimate strength in the engineering stress–strain curve [3]. After this point, the true stress drops to a new value of stress which is called damaged stress and the damage evolution starts to accumulate after the point of ultimate stress. The damage variable (D) is the measured parameter that can describe the amount of damage after damage initiation. At the onset of necking, the damage variable D is equal to zero but the ductile damage initiation criteria (ω_D) reaches the critical value = 1 [5]. At complete fracture, the damage variable (D) is equal to an experimental value which can be specified to (D_f). This model also proposes that the damage initiation criteria depend on strain rate, stress triaxiality, and forming temperature.

Bridgman [6], Davidson and Ansell [7] proved a relation between ductility and pressure (P). McClintock [8] and Rice and Tracey [9], deduced an expression relating between the stress triaxiality and the strain to fracture by a study of the void growth. The damage proposed occurs when the plastic strain causes a local instability in the form of localized strain bands [10, 11]. Bai et al. considered the studies of void growth as the basis of the modern ductile fracture mechanics [12, 13]. Bao [14] proved that increasing the stress triaxiality decreases the fractural strain for Steel C45. Mohanraj et al. [15] proved that increasing the stress triaxiality decreases the complete fractural strain for steel C45 by using notched specimens to show the effect of stress triaxiality.

The temperature and strain rate effects on damage strains were studied by Johnson and Cook [16] and Johnson and Holmquist [17] using the Split-Hopkinson tension-bar test on AISI 4340 steel to prove a model containing three brackets that cover the effect of temperature (linear function), strain rate effect (logarithmic function), and stress triaxiality effect (exponential function). This model contains five constants that need to be determined for each material (model calibration). Abed et al. [18, 19] used coupled model which consisted of J-C strength model and energy model to express the damage at different temperatures and different strain rates using microscopic scans for the fractured specimens during tensile test. Su-Tang et al. [20] studied the effect of strain rate and temperature on flow stress and complete fractural strain by using tensile test data.

Obviously, the damage data has been obtained historically from tensile tests, which not only represent the uniaxial state but also can represent multi-axial state using notched specimens with different radii to control the stress triaxiality. This makes the obtained data valid for complex metal forming processes as forging, bending, and deep drawing.

In this paper, a trial to create trends and statistical models to express the effects of the forming conditions on the damage behavior using the stress–strain curves of steel C45 as a material case study. Therefore, in this work, the damage behaviors were obtained conventionally-from tensile test results carried out on un-notched specimens at different temperatures and strain rates [20] and tensile tests carried out on notched specimens on steel C45 [15].

2 Problem Description and Motivation

During any hot forging process (especially, for the complex shape products), some surface cracks may be nucleated. Therefore, the motivation of this work is determining relations between the forming conditions (forming temperature, forming strain rate, and forming stress triaxiality) and crack nucleation parameter that is expressed as the plastic strain at damage initiation and the fractural plastic strain. Also, this work aims to obtain the trends that relate the forming parameters with the damage initiation strain and fractural strain. Also, it is a trial to create statistical models to relate the damage strains (damage initiation strain and fractural strain) to the forming parameters. Thus; these models can predict (forecast) the forming conditions (out of experimental data) that may cause these crakes.

3 Methodology

The methodology which was used to achieve the previous aim of this work is, first, specifying a suitable damage model which can deal with the hot forging process. The most suitable model is the ductile damage model that involves obtaining the plastic strain at damage initiation. According to (2) and (3), the damage starts at the necking zone that starts to form at the engineering ultimate point due to voids nucleation until complete fracture at voids coalescence. Therefore the way in determining the ultimate and fractural points from engineering curves using Eqs. (1) and (2) therefore, deducing the damage initiation strains (corresponding to ultimate point) and fractural strains (corresponding to fractural endpoint) at the different forming conditions by using the Eq. (3). The experimental stress–strain curves for C45 steel-as a case study- were available in [15, 18]. The results of true plastic strain at engineering ultimate point and at fractural point were analyzed and plotted against the different forming conditions to obtain the effect of these forming conditions on damage strains and stresses including general trends and approximated statistical models which can

relate them. These models can predict the damage initiation strain and fractural strain at other forming conditions which were out of the available experimental data and inside the experimental range.

$$\sigma_{\text{eng.}} = \frac{\sigma_{\text{true}}}{1 + \varepsilon_{\text{eng.}}} \quad (1)$$

$$\varepsilon_{\text{eng.}} = (e^{\varepsilon_{\text{true}}} - 1) \quad (2)$$

$$\varepsilon^{\text{pl}} = \varepsilon_{\text{true}} - \frac{\sigma_{\text{true}}}{E} \quad (3)$$

$$d_c = L_c \left(\varepsilon_f^{\text{pl}} - \varepsilon_0^{\text{pl}} \right) \quad (4)$$

where

$\sigma_{\text{eng.}}$	Engineering Stress
σ_{true}	True Stress
E	Young's Modulus
ε^{pl}	True Plastic Strain
ε_{eng}	Engineering Strain
$\varepsilon_{\text{true}}$	True Strain
$\varepsilon_f^{\text{pl}}$	True plastic strain at fracture
$\varepsilon_0^{\text{pl}}$	True plastic strain at ultimate.

At constant stress triaxiality, the experimental stress–strain data at temperatures range (from 298 to 923 °K), and different strain rates (from 0.0015 to 885 S⁻¹) for steel C45 were extracted from Ref. [18] using Get data Graph Digitizer software. However, the data which study the stress triaxiality effect were extracted from another review [15] as a (stress triaxiality–fractural strain) curve at room temperature.

At constant stress triaxiality: the engineering stress–strain data were calculated using Eqs. (1) and (2) leading to determination of engineering ultimate points strain and engineering fractural points strain which was transformed into the plastic true one using Eq. (3) to get; damage initiation strain, $\varepsilon_0^{\text{pl}}$, damage fractural strain, $\varepsilon_f^{\text{pl}}$, and the element displacement ratio. True plastic strain difference between the damage fracture strain and initial damage strain was calculated using Eq. (4).

4 Results Analysis and Discussion

4.1 Engineering Ultimate and Fractural Point's Results

Engineering stress–strain curves were obtained using Eqs. (1) and (2) and, the results were summarized in Table 1.

Table 1 Engineering ultimate and fractural points at different temperatures and strain rates

Strain rate	Temperature	Engineering ultimate point		Engineering fracture point	
		Stress	Strain	Stress	Strain
0.0015	298	844.3673	0.0481	759.1095	0.0890
	523	836.9600	0.0556	687.0961	0.1163
	723	509.3845	0.0445	259.1772	0.1238
	923	201.0202	0.0432	45.9844	0.2668
0.015	298	874.0914	0.0476	824.2929	0.0796
0.15	298	926.4845	0.0515	921.5375	0.0623
	523	833.9754	0.0613	754.9342	0.0779
	723	702.6436	0.0587	515.5113	0.1252
	923	293.0745	0.0460	145.9961	0.2609

4.2 Forming Temperature Effect

The influence of forming temperature on the damage initiation strain (ϵ_0^{pl}) and fractural strains (ϵ_f^{pl}) can be expressed by different trends as follows.

4.2.1 Damage Initiation Strain at Different Temperatures

The values of damage initiation strains at different temperatures were calculated using Eq. (3) and summarized in Table 2. The results were plotted to represent the temperature effect on damage initiation strain and corresponding true stresses at engineering ultimate point as shown in Figs. 1 and 2.

Table 2 True plastic strains and true stresses at damage initiation

Strain rate	Temperature	True plastic strain at damage initiation	True stress at engineering ultimate point
0.0015	298	0.0349	885.0000
	523	0.0266	883.4951
	723	0.0232	532.0388
	923	0.0200	209.7087
0.15	298	0.0382	974.2389
	523	0.0331	885.1300
	723	0.0328	743.8933
	923	0.0250	306.5495

Fig. 1 The forming temperature effect on the damage initiation strain

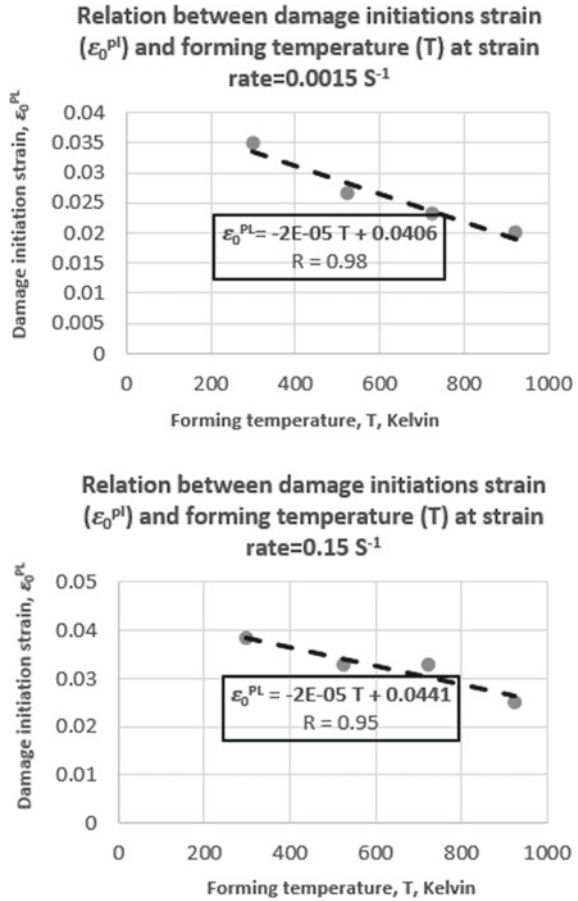
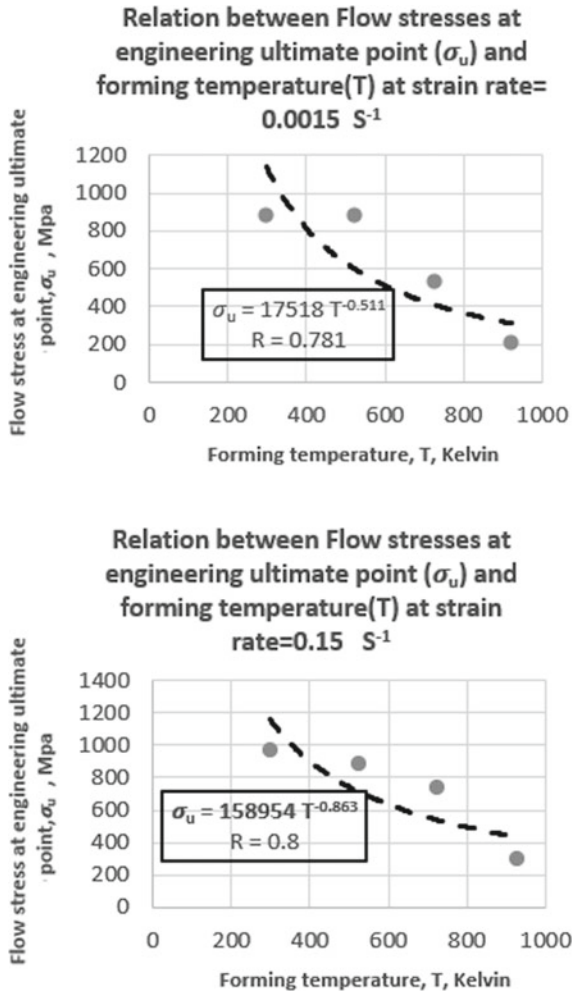


Figure 1 shows the relationship between the damage initiation strain (ϵ_0^{pl}) and forming temperature (T). It can be represented by proportional inverse linear relationship. The influence of the formation temperature on the flow stress at the ultimate point (σ_u) was shown in Fig. 2. This relationship can be expressed as an inverse power relationship.

This reverse relationship between forming temperature and the strain at the onset of damage (voids nucleation) may be physically explained based on that the increase in the temperature enlarges the grain size which makes the void formation about it more readily (2). Once the voids are nucleated, the necking (damage initiation) starts (Sect. 1). Also, the temperature rising increases the activation energy which can overcome the cohesion between the material matrix and the second phase grains (act as impurities or inclusions in steels). Therefore, this creates free surfaces around the second phase (2) where the voids are nucleated. Hence, the damage starts to occur. The two previous reasons explain the small strain which occurs before the onset

Fig. 2 The forming temperature effect on the flow stress at engineering ultimate point



of damage when the forming temperature rises. Also, this may clarify the reason for decreasing the ultimate strength due to interface decohesion between grains, therefore the bonding force decreases.

4.2.2 Fractural Strain at Different Temperatures

The values of fractural strains at different temperatures were calculated using Eq. (3) and summarized in Table 3 therefore the results were plotted in Figs. 3 and 4.

The influence of forming temperature (T) on the fractural strain (ϵ_f^{pl}) behavior was presented in Fig. 3. It can be expressed as a direct linear proportional relationship.

Table 3 Forming temperature effect on true plastic strain and true stress at complete failure

Strain rate	Temperature	True plastic strain at complete failure	True plastic strain difference	True stress at fracture
0.0015	298	0.0740	0.0391	826.6979
	523	0.0861	0.0595	766.9903
	723	0.1056	0.0824	291.2621
	923	0.2303	0.2103	58.2524
0.15	298	0.0483	0.0101	978.9227
	523	0.0507	0.0176	813.7300
	723	0.0990	0.0663	580.0613
	923	0.2198	0.1948	184.0824

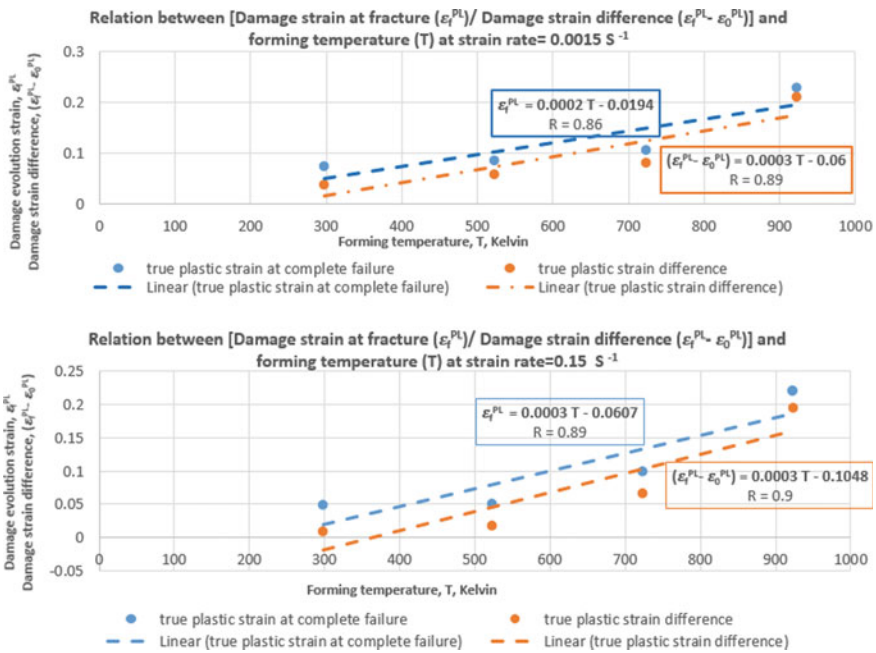


Fig. 3 The forming temperature effect on the fractural strain behavior

Figure 3a represents the fractural strain (ϵ_f^{pl}) at strain rate (0.0015 S⁻¹) but Fig. 3b indicates the fractural strain (ϵ_f^{pl}) at strain rate (0.15 S⁻¹). The influence of forming temperature (T) on the fractural flow stress (σ_f) is presented in Fig. 4 and can be presented by a reverse power relationship.

The results of the forming temperature (T) and fractural strain (ϵ_f^{pl}) may be explained starting from that, in general, the voids—which previously were deformed—grow under the effect of hydrostatic stress and further strain until the

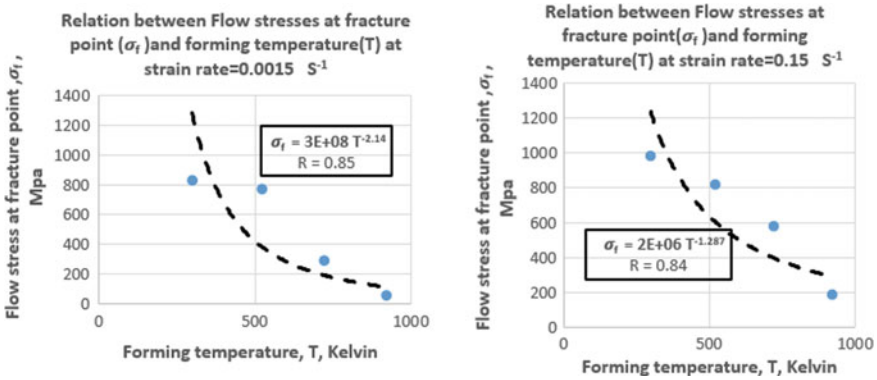


Fig. 4 The forming temperature effect on the fractural flow stress

coalescence occurs (complete fracture). However, with the temperature increasing, the grain size increases under the effect of hydrostatic stress and temperature. This increase in the grain size may overcome the void growth around the grain, therefore restricting the coalescence effect (as a barrier). Also increasing the temperature increases the ductility which exhibits larger strains in grains than in voids. This may explain the large strain before coalescence occurs (complete fracture).

The statistical models which describe the temperature effect were summarized in Table 4.

The results of fractural strain agree –in trend type- with the results obtained by Chiou et al. [19]. Also, the fractural stress results were obtained by Reza et al. [21].

The obtained statistical models are in agreement with the temperature term in Johnson–Cook damage model [16] and Johnson–Cook strength model. The above models were concluded at two strain rates (0.0015 and 0.15 S⁻¹) and at the temperature range from 298 to 923 °K.

Table 4 The statistical models which relate the forming temperature with damage strains and stresses at $T = 298^\circ, 523^\circ, 723^\circ,$ and 923°K on two different strain rates

Dependent parameter	Strain rate (S ⁻¹)	
	0.0015	0.15
ϵ_0^{PL}	$\epsilon_0^{PL} = -0.00002T + 0.0406$	$\epsilon_0^{PL} = -0.00002T + 0.0441$
ϵ_f^{PL}	$\epsilon_f^{PL} = 0.0002T - 0.0194$	$\epsilon_f^{PL} = 0.0003T - 0.0607$
$(\epsilon_f^{PL} - \epsilon_0^{PL})$	$(\epsilon_f^{PL} - \epsilon_0^{PL}) = 0.0003T - 0.06$	$(\epsilon_f^{PL} - \epsilon_0^{PL}) = 0.0003T - 0.1048$
σ_u	$\sigma_u = 17,518T - 0.511$	$\sigma_u = 158,954T - 0.863$
σ_f	$\sigma_f = 3(10)^8 T - 2.14$	$\sigma_f = 2(10)^6 T - 1.287$

Table 5 Strain rate effect on true plastic strain and true stress at damage initiation at different temperatures

Temperature	Strain rate	True plastic strain at damage initiation	True stress at engineering ultimate point
298	0.0015	0.0349	885.0000
	0.015	0.0352	915.6909
	0.15	0.0382	974.2389
	620	0.0193	1185.7296
	767	0.0200	1205.7869
	885	0.0274	1266.1206
523	0.0015	0.0266	883.4951
	0.15	0.0331	885.1300
723	0.0015	0.0232	532.0388
	0.15	0.0328	743.8933
923	0.0015	0.0200	209.7087
	0.15	0.0250	306.5495

4.3 Strain Rate Effect

The strain rate affected the damage initiation strain ($\varepsilon_0^{\text{pl}}$) and the damage evolution strain $\varepsilon_f^{\text{pl}}$ by different trends as following later.

4.3.1 Damage Initiation Strain at Different Strain Rates

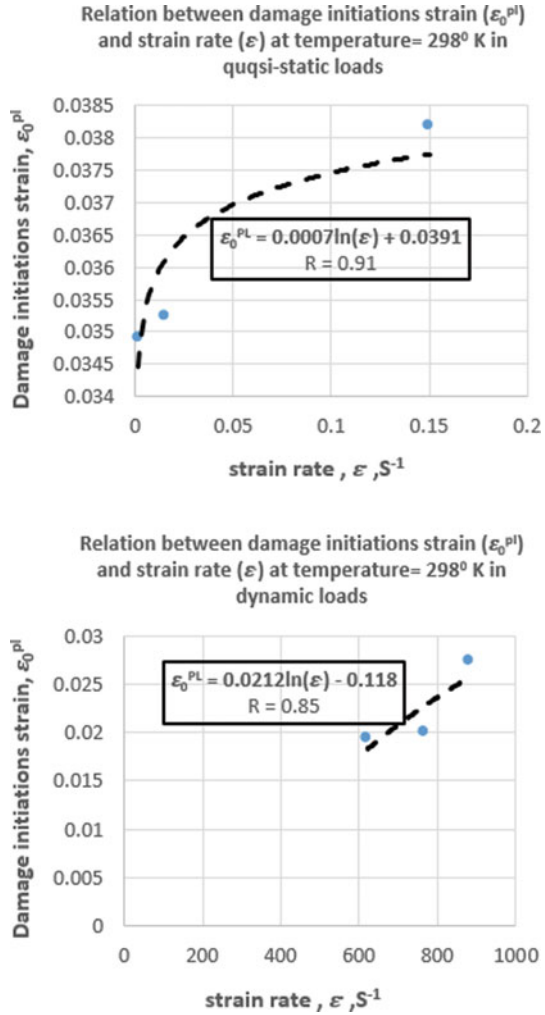
The values of damage initiation strains at different temperatures were calculated using Eq. 3 and summarized in Table 5. The results were plotted to show the temperature effect as shown in Figs. 5 and 6.

Figure 5 shows the relationship between strain rate and the damage initiation strain ($\varepsilon_0^{\text{pl}}$) at constant formation temperature (298 K). It can be noticed that there is a direct proportional logarithmic relationship. The influence of the strain rate on the flow stress at the geometric endpoint is shown in Fig. 6. This relationship can be expressed as a direct proportional as logarithmic relationship.

4.3.2 Fractural Strain at Different Strain Rates

The values of fractural strains ($\varepsilon_f^{\text{pl}}$) at different strain rates were calculated using Eq. (3) and summarized in Table 6. The results were plotted in Fig. 7. The relationship between strain rate and fractural strain is shown in Fig. 7. In general, these relations can be expressed as inversely proportional logarithmic functions. Figure 7a represents

Fig. 5 The effect of strain rate on the damage initiation strain at $T = 298\text{ }^\circ\text{K}$ in the quasi-static and dynamic loads

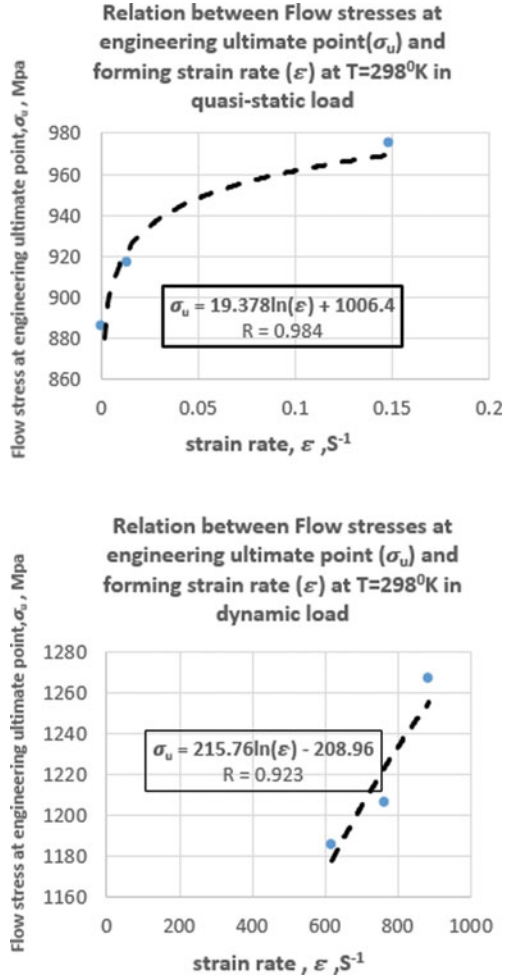


the fractural strain (ϵ_f^{pl}) at quasi-static test and Fig. 7b indicates the fractural strain (ϵ_f^{pl}) at dynamic tests.

The relationship between strain rate and fractural strain is shown in Fig. 7. In general, these relations can be expressed as inversely proportional logarithmic functions. Figure 7a represents the fractural strain (ϵ_f^{pl}) at quasi-static test and Fig. 7b indicates the fractural strain (ϵ_f^{pl}) at dynamic tests.

Figure 8 shows the strain rate ($\dot{\epsilon}$) effect on the fractural flow stress. It can be noticed that the relation between the forming strain rate ($\dot{\epsilon}$) and the true stress at ultimate (σ_u) and fractural (σ_f) points are relatively direct proportional and can be expressed by logarithmic function as summarized in Table 7. Table 7 Shows the

Fig. 6 The effect of strain rate on the flow stress at the engineering ultimate point at $T = 298 \text{ }^\circ\text{K}$ in the quasi-static and dynamic loads



statistical models which relate forming strain rate with damage strains and stresses at $T = 298 \text{ }^\circ\text{K}$ on two groups of strain rates.

The reverse relation between fractural strain (ϵ_f^{pl}) and strain rate perhaps due to the high velocity in forming which may cause high dynamic energy that can produce high hydrostatic pressure which fastens the growth and coalescence of voids.

The previous results of strain rate effects correspond—in function type—with [16]. Also the results of fractural strain and fractural stress match—in trend type—with the results obtained by Woei-Shyan and Chou [22]. As well, the fractural stress results coincide with the results conducted by Reza et al. [21]. Also, the ultimate stress results match with the results gained by Lin and Liu [23] but the results of ultimate and fractural stresses are in agreement with the results taken out by Chiou et al. [19].

Table 6 True plastic strain and true stress values at complete failure at different strain rates

Temperature	Strain rate	True plastic strain at complete failure	True plastic strain difference	True stress at fracture
298	0.0015	0.0740	0.0357	826.6979
	0.015	0.0657	0.0304	889.9297
	0.15	0.0483	0.0101	978.9227
	620	0.2839	0.2646	185.7612
	767	0.2554	0.2354	349.1729
	885	0.2465	0.2191	449.5790
523	0.0015	0.0861	0.0595	766.9903
	0.15	0.0507	0.0176	813.7300
723	0.0015	0.1056	0.0824	291.2621
	0.15	0.0990	0.0663	580.0613
923	0.0015	0.2303	0.2103	58.2524
	0.15	0.2198	0.1948	184.0824

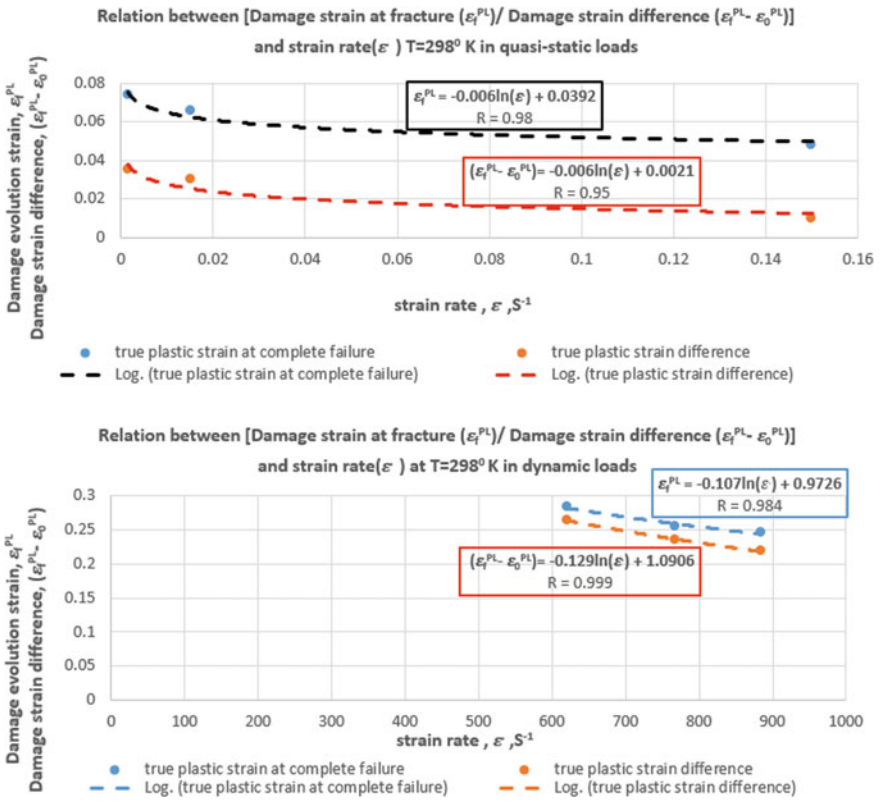


Fig. 7 The strain rate effect on the fractural strain behavior

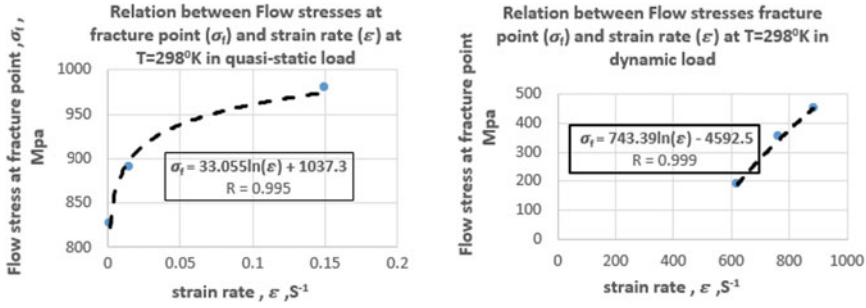


Fig. 8 The strain rate effect on the fractural flow stress

Table 7 Statistical models which relate forming strain rate with damage strains and stresses

Dependent parameter	Temperature (K)	
	298 °K (at: strain rates = 0.0015, 0.015, and 0.15 S ⁻¹)	298 °K (at: strain rates = 620,767, and 885 S ⁻¹)
ϵ_0^{PL}	$\epsilon_0^{PL} = 0.0007 \ln(\epsilon) + 0.0391$	$\epsilon_0^{PL} = -0.00002T + 0.0441$
ϵ_f^{PL}	$\epsilon_f^{PL} = -0.006 \ln(\epsilon) + 0.0392$	$\epsilon_f^{PL} = -0.107 \ln(\epsilon) + 0.9726$
$(\epsilon_f^{PL} - \epsilon_0^{PL})$	$(\epsilon_f^{PL} - \epsilon_0^{PL}) = -0.006 \ln(\epsilon) + 0.0021$	$(\epsilon_f^{PL} - \epsilon_0^{PL}) = -0.129 \ln(\epsilon) + 1.0906$
σ_u	$\sigma_u = 19.378 \ln(\epsilon) + 1006.4$	$\sigma_u = 215.76 \ln(\epsilon) - 208.96$
σ_f	$\sigma_f = 33.055 \ln(\epsilon) + 1037.3$	$\sigma_f = 743.39 \ln(\epsilon) - 4592.5$

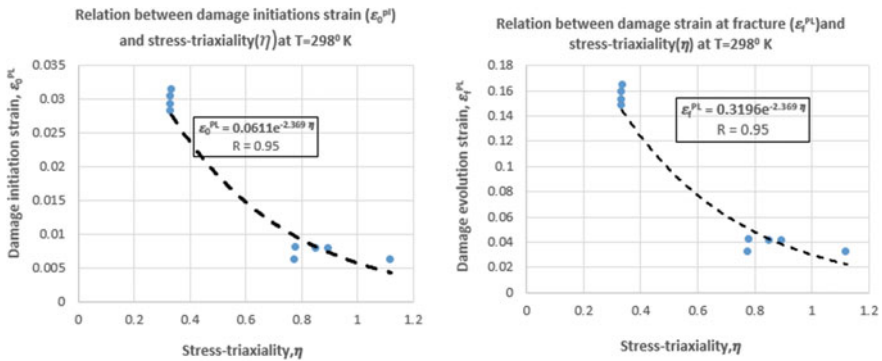


Fig. 9 The effect of stress-triaxiality on damage initiation strain and fractural strain at T = 298 °K

Table 8 Statistical models relate the forming stress triaxiality with damage strains

Dependent parameter	Temperature(K)
	298 °K
ϵ_0^{PL}	$\epsilon_0^{PL} = 0.0611 e^{-2.369\eta}$
ϵ_f^{PL}	$\epsilon_f^{PL} = 0.3196e^{-2.369\eta}$

4.4 Stress Triaxiality Effect

Figure 9 indicates that the relation between the forming stress triaxiality (η) and the damage initiation strain (ϵ_0^{pl}) and the fractural strain (ϵ_f^{pl}) is inverse proportional by exponential functions.

This reverse relation between stress triaxiality and the fractural strains may be explicated based on the definition of stress triaxiality which is the ratio between the average of the principal stresses (σ_m) and the equivalent Von-Mises stress (σ_e). The increasing of this ratio means increasing (σ_m) and/or decreasing (σ_e). This may be achieved by high positive three principal stresses ($\sigma_1, \sigma_2, \sigma_3$) which leads to interface decohesion between pre-existing second phase and the material matrix.

The statistical models which relate the forming stress triaxiality with damage strains at $T = 298 \text{ °K}$ were summarized in Table 8.

These statistical models are similar to stress triaxiality term in Johnson–Cook damage model [16] and similar to the model proved by Bai [14].

4.4.1 Finite Element Case Study (on Stress Triaxiality Effect)

This case study aims to show and simulate the effect of stress triaxiality on the damage criteria.

A. Modeling Procedure

The model was designed on a specimen with the shown geometry and in Fig. 10. The material was described elastically and plastically. The damage initiation strain and fractural strain were defined at different stress triaxiality (Sect. 4.4). The lower cell was set as fully constrained but the upper one was set to be free in the axial direction. First, the meshing size optimization was conducted to determine a suitable size of the elements.

B. Damage Criteria Results

The visualization results of the artificial tensile test were focused on the first elements which reached the critical value of damage criteria (Figs. 11 and 12). The value of ductile damage criteria for this damaged element was assigned to the corresponding values of axial plastic strain and the stress triaxiality in the time domain (Figs. 13 and 14). Also, the effect of damage on the strength of this element was clarified (Fig. 15).

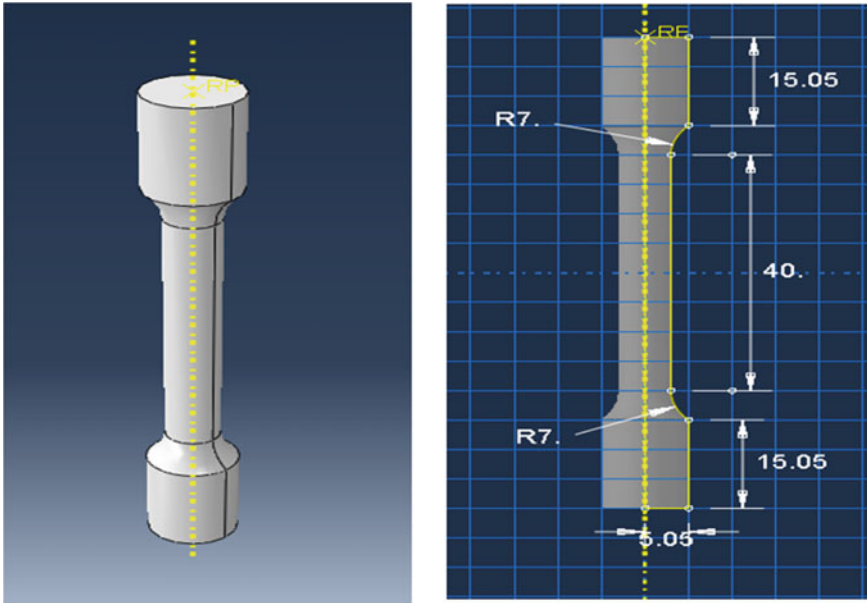


Fig. 10 The geometry and dimensions of the specimen

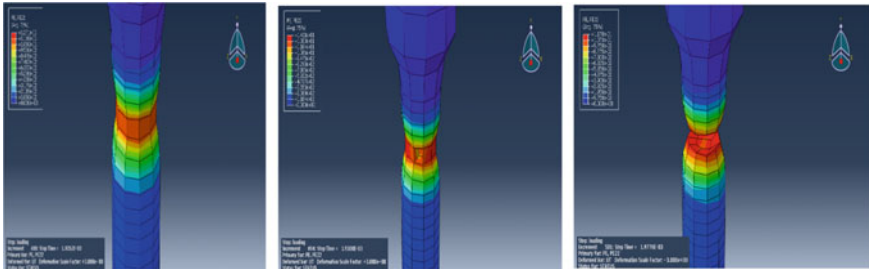


Fig. 11 The visualization results of the tensile test

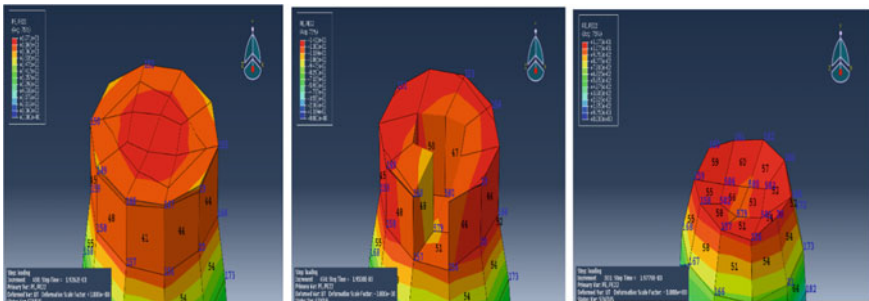


Fig. 12 The visualization results at a cutting plane passes through the removed elements (41, 43, and 46)

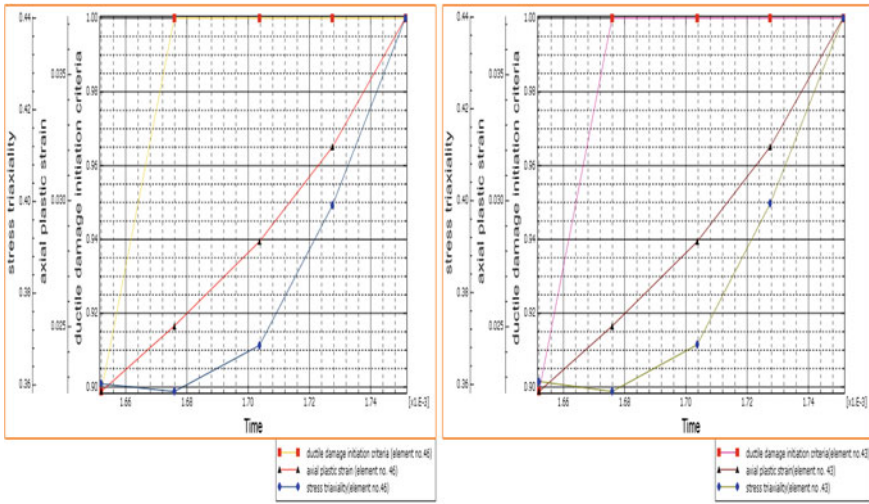


Fig. 13 The first two elements (43 and 46) which reaches the critical value of damage initiation criteria

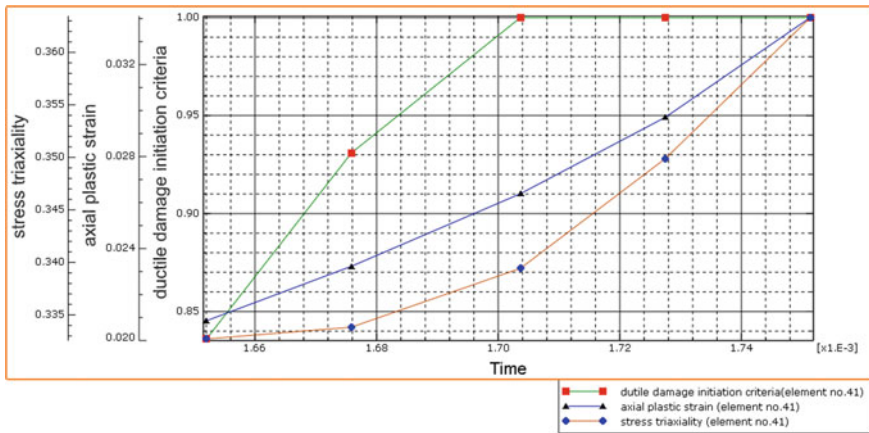


Fig. 14 The third element which reaches the critical value of damage initiation criteria

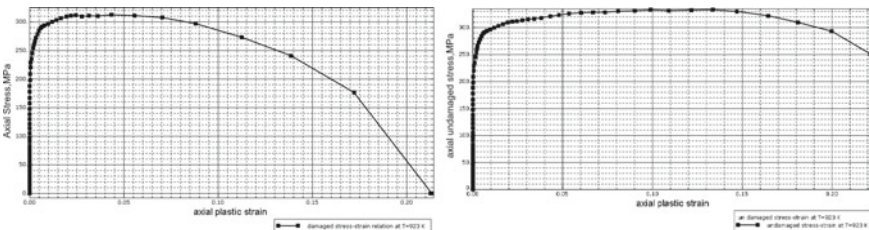


Fig. 15 The effect of damage on the strength values for elements (43 and 46)

(1) Stress Triaxiality Effect on Damage Criteria

Figures 11a and 12a show all elements before damage at a cutting plane passes through the removed elements but Figs. 11b and 12b show the first three removed elements which reach the critical values of damage criteria. Figures 11c and 12c clear that all the other elements of this section were removed soon later. Therefore, outputs of this model (damage initiation criteria, stress triaxiality, and plastic strain) were extracted from the field outputs in time domain to clear and explain the previously mentioned shortage. Therefore, these results were plotted against time (Figs. 14 and 15) for the three elements.

Figure 13 demonstrates the first two elements (43 and 46) reached the critical value of the damage initiation criteria at time equal to $1.677\text{E-}3$ s., stress triaxiality equal to 0.36, and axial plastic strain equal to 0.025 but Fig. 14 shows that the third element (41) reached the critical value of the damage initiation criteria at time equal to $1.71\text{E-}3$ s., stress triaxiality equal to 0.339, and axial plastic strain equal to 0.0265. At the first time ($1.677\text{E-}3$ s.), the third element (41) was at stress triaxiality equal to 0.33 which is smaller than its value (0.36) for elements (43 and 46).

These results may be explained based on that the first two elements (43 and 46) are central elements in the section and are bounded by other elements. This increases the pressure on them more than the edge circumferential elements which have free surfaces, therefore these central elements have a higher value of stress triaxiality. This makes them more prepared for damage initiation. This explanation may agree with the statistical inverse exponential function in Table 8. This may explain the cup-cone fractural shape in the necking zone.

(ii) Damage Effect on Strength

Figure 15a clarifies that the damage began at axial plastic strain equal to 0.025 and the full fracture (zero stress) occurred at axial plastic strain equal to 0.21. The accumulation of damage started from strain 0.025 until strain 0.21(fracture).this accumulation reduced the strength values after strain 0.025 but Fig. 15b shows that after this strain (0.025) the strength increased as usual in case of neglecting the damaging effect.

This result can be interpreted as a result of stiffness degradation in the material matrix due to the void growth and interface decohesion.

5 Conclusions

1. Increasing forming temperature increases the fracture plastic strain and the displacement after the damage initiation until the fracture. At the same time reduces the true stress at ultimate and fracture points and reduces the damage initiation plastic strain.
2. Increasing the forming strain rate decreases the fracture plastic strain and the displacement after the damage initiation until the fracture occurs.

3. Increasing in the forming stress triaxiality decreases the fractural strain and the damage initiation strain.
4. The statistical models obtained in this paper have the same types of function which were proved by Johnson and Cook in their constitutive models (strength and damage models).
5. The finite element models may help in determining the location of the first damage in the necking zone where the higher stress triaxiality exists.

References

1. Meyers MA (2002) Constitutive description of dynamic deformation: physically-based mechanisms. *Mater Sci Eng A* 322:194–216
2. Anderson TL (2008) *Fracture mechanics—Fundamentals and applications*, 3rd edn. Taylor & Francis
3. Callister WD, Rethwisch DG (2010) *Fundamentals of materials science and engineering*, 4th edn.
4. Tvergaard V (1982) On localization in ductile materials containing spherical voids. *Int J Fract* 18(4):237–252
5. Abaqus/CAE user's manual, version 6.14 edition
6. Bridgman PW (1952) *Studies in large plastic flow and fracture*, vol 177. McGraw-Hill, New York
7. Davidson T, Ansell G (1968) The structure sensitivity of the effects of pressure upon the ductility of Fe-C materials. *ASM Trans Quart* 61(2):242–254
8. McClintock FA (1968) A criterion for ductile fracture by the growth of holes. *J Appl Mech* 35(2):363–371
9. Rice JR, Tracey DM (1969) On the ductile enlargement of voids in triaxial stress fields. *J Mech Phys Solids* 17(3):201–217
10. Gurson AL (1977) Continuum theory of ductile rupture by void nucleation and growth: Part I—Yield criteria and flow rules of porous ductile media. *J Eng Mater Technol* 99:2–15
11. Tvergaard V (1989) Material failure by void growth to coalescence. *Adv Appl Mech* 27:83–151
12. Bai Y, Teng X, Wierzbicki T (2009) On the application of stress triaxiality formula for plane strain fracture testing. *J Eng Mater Technol* 131(2)
13. Bai Y, Wierzbicki T (2008) A new model of metal plasticity and fracture with pressure and Lode dependence. *Int J Plast* 24(6):1071–1096
14. Bai Y, Wierzbicki T (2005) On the cut-off value of negative triaxiality for fracture. *Eng Fract Mech* 72(7):1049–1069
15. Murugesan M, Jung DW (2019) Johnson Cook material and failure model parameters estimation of AISI-1045 medium carbon steel for metal forming applications. *Materials* 12:609
16. Johnson GR, Cook WH (1983) A constitutive model and data for metals subjected to large strains, high strain rates and high temperatures. In: Paper presented in the proceedings of the 7th international symposium on ballistics, pp 541–547
17. Johnson GR, Holmquist T (1989) Test data and computational strength and fracture model constants for 23 materials subjected to large strains, high strain rates, and high temperatures. Los Alamos National Laboratory, Los Alamos, NM, Report No. LA-11463-MS
18. Abed FH, Saffarini MH, Abdul-Latif A, Voyiadjis GZ (2017) Flow stress and damage behavior of C45 steel over a range of temperatures and loading rates. *J Eng Mater Technol Trans ASME* 139:1–8.
19. Chiou S-T, Tsai H-L, Lee W-S (2007) Effects of strain rate and temperature on the deformation and fracture behavior of titanium alloy. *Mater Trans Jpn Inst Metals* 48(9):2525–2533

20. Abed FH, Abdul-Latif A, Yehia A (2018) Experimental study on the mechanical behavior of EN08 steel at different temperatures and strain rates. *Metals* 8:736
21. Ferdowsi MRG, Nakhaie D, Benhangi PH, Ebrahimi GR (2014) Modeling the high temperature flow behavior and dynamic recrystallization kinetics of a medium carbon microalloyed steel". *JMEPEG ASM Int* 23:1077–1087
22. Lee W-S, Chou J-K (2005) The effect of strain rate on the impact behavior of Fe-2 mass% Ni sintered alloy. *Mater Trans Jpn Inst Metals* 46(4):805–811
23. Lin YC, Liu G (2010) A new mathematical model for predicting flow stress of typical high-strength alloy steel at elevated high temperature. *Comput Mater Sci* 48(54):58